Journal of Microscopy

Journal of Microscopy, Vol. 00, Issue 0 2018, pp. 1–9
Received 30 April 2018; accepted 13 July 2018

doi: 10.1111/jmi.12747

Cryofixation during live-imaging enables millisecond time-correlated light and electron microscopy

M. FUEST*, G. M. NOCERA*, M. M. MODENA, D. RIEDEL, Y. X. MEJIA & T. P. BURG
Max Planck Institute for Biophysical Chemistry, Goettingen, Germany

Key words. Correlative microscopy, cryofixation, microfluidics.

Summary

Correlating live-cell imaging with electron microscopy is among the most promising approaches to relate dynamic functions of cells or small organisms to their underlying ultrastructure. The time correlation between light and electron micrographs, however, is limited by the sample handling and fixation required for electron microscopy. Current cryofixation methods require a sample transfer step from the light microscope to a dedicated instrument for cryofixation. This transfer step introduces a time lapse of one second or more between live imaging and the fixed state, which is studied by electron microscopy. In this work, we cryofix *Caenorhabditis elegans* directly within the light microscope field of view, enabling millisecond time-correlated live imaging and electron microscopy. With our approach, the time-correlation is limited only by the sample cooling rate. *C. elegans* was used as a model system to establish compatibility of *in situ* cryofixation and subsequent transmission electron microscopy (TEM). TEM images of *in situ* cryofixed *C. elegans* show that the ultrastructure of the sample was well preserved with this method. We expect that the ability to correlate live imaging and electron microscopy at the millisecond scale will enable new paradigms to study biological processes across length scales based on real-time selection and arrest of a desired state.

Introduction

Correlative light and electron microscopy (CLEM) is among the most promising approaches to study functions of cells and small organisms across length scales (Plitzko *et al.*, 2009; de Boer *et al.*, 2015; Loussert Fonta & Humbel, 2015). CLEM bridges the resolution gap by first using light microscopy to map specific organelles and proteins at the cellular level and then using electron microscopes to visualise ultrastructure in the cellular context. Although CLEM refers to the correlation of a wide variety of light and electron microscopy techniques, correlating live imaging with electron microscopy (EM) allows dynamic functions at the cellular or organism level to be related to the underlying ultrastructure. Current methods to correlate live imaging with EM, however, suffer from limited time resolution due to the fixation and sample preparation required prior to EM. Here we demonstrate the time lapse between live imaging and sample immobilisation for EM can be reduced from a limit of seconds to milliseconds by conducting high-quality cryofixation directly in the light microscope field of view.

Cryofixation is widely accepted as the gold-standard fixation method for high-resolution imaging, most notably (cryo)electron microscopy and tomography (Gautier *et al.*, 1986; McDonald & Morphew, 1993; Müller-Reichert *et al.*, 2003; Al-Amoudi *et al.*, 2004; Brown *et al.* 2009; Dubochet, 2012; Schertel *et al.*, 2013; Schaffer *et al.*, 2017). High-pressure freezing and plunge freezing have been the cryofixation methods of choice since the 1980s (Moor & Riehle, 1968; Dubochet & McDowall, 1981; Moor, 1987); however, these methods place a limitation on CLEM time resolution. After a region and time of interest is located in the light microscope, the sample must be transferred to a dedicated instrument for cryofixation (i.e. high-pressure or plunge freezing system). The transfer step introduces a time lapse between live imaging and the fixed state, which is studied by electron microscopy. Development of automated systems (Verkade, 2008; Koning *et al.*, 2014), some of which are now commercially available, minimised this time lapse to 1–5 s, though preparation times up to a few minutes are still common (McDonald, 2009; Plitzko *et al.*, 2009; Koning *et al.*, 2014).

Current approaches carefully time cryofixation to occur at a known time interval following user-initiation of a certain dynamic process or perturbation. Such methods have allowed electron microscopy studies to provide snapshots of dynamic processes with a time resolution of ~10 ms (Heuser *et al.*, 1979; Wendt-Gallitelli & Wolburg, 1984; Knoll *et al.*, 1991; Ménétret *et al.*, 1991). However, these techniques do not allow direct correlation between live imaging and electron microscopy.

* These authors contributed equally to this work.
Correspondence to: Thomas P. Burg, Max Planck Institute for Biophysical Chemistry, Am Fassberg 11, 37077 Goettingen, Germany. Tel: +49 551 201-1187; fax: +49 551 201-1577; e-mail: tburg@mpibpc.mpg.de

Innovative design modifications have been introduced to both the high-pressure and plunge freezer to facilitate cryofixation timing. Plunge freezing is commonly used to prepare ultra-thin (<100 nm) vitrified layers of purified single particles (ribosomes, proteins, viruses etc.) for structural studies by cryo-EM. High-pressure freezing is used to preserve the ultrastructure of larger samples, such as whole cells and small organisms. For specific questions in cellular dynamics, where the process of interest can be triggered using optogenetics or electrical stimulation, specially modified high-pressure freezers (such as the Leica EM ICE) have been developed to trigger select responses just tens of milliseconds prior to cryofixation (Watanabe *et al.*, 2013). Unfortunately, many dynamic processes cannot be artificially initiated (Shaikh *et al.*, 2009; Chen & Frank, 2016; Stepanek & Pigino, 2017), limiting applicability of this method.

Currently there are no techniques available that allow direct correlation of live imaging and electron microscopy with millisecond time resolution. Therefore, the state of each individual specimen must be inferred postfixation. Some information, such as directionality leading up to fixation, crucial for investigations of, for example, intracellular transport (Stepanek & Pigino, 2017), is lost entirely. Live imaging milliseconds before cryofixation would open the possibility to reproducibly investigate rare, directional, or highly dynamic processes that occur on the timescale of milliseconds.

In this work, we demonstrate millisecond time-correlated live imaging and transmission electron microscopy (TEM), enabled by cryofixing the sample directly within the field of view of the light microscope. We used the roundworm *Caenorhabditis elegans* as a model system to show that (i) the *in situ* cryofixation technology is capable of revealing a well-preserved ultrastructure in EM and (ii) the procedure is compatible with established sample preparation techniques for electron microscopy. With this newly developed approach (Fig. 1), the time correlation of live imaging and electron microscopy is limited only by the sample cooling rate to the order of milliseconds.

Results

Integrated light microscopy and cryofixation

The working principle of the *in situ* cryofixation system relies on conductive heat transfer. A PDMS (polydimethylsiloxane) microchannel is mounted onto a thin film resistive heater (Fig. 1). The heater is placed in thermal contact with a liquid nitrogen (LN_2) cooled heat sink. The heater maintains the sample in the microchannel at room temperature during live imaging. At the desired moment, the power to the heater is turned off. The sample cools rapidly and is cryofixed within the light microscope field of view.

The distance between the sample and the heat sink (marked by a red line in Fig. 1) is the most critical parameter influencing the cooling rate, and thus the quality of the sample preservation (Studer *et al.*, 1995). In this work, this distance ranges from ~27 μm to 40 μm depending on the location of the sample within the 25 μm channel depth. The total size of the channel, including all four PDMS walls, is limited to ~70 μm × 130 μm × 1.7 mm to minimise the amount of

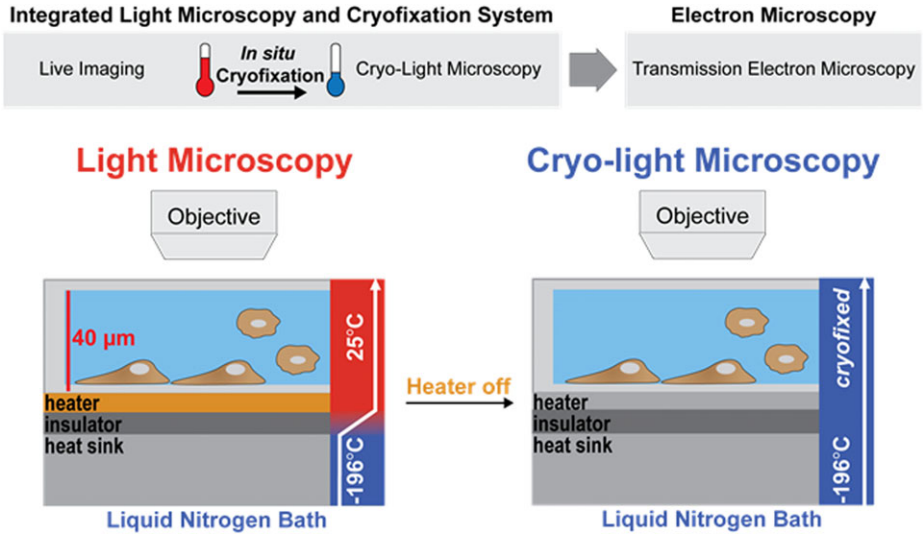

Fig. 1. Connecting in situ cryofixation to electron microscopy enables millisecond time-correlated live imaging and electron microscopy. The *in situ* cryofixation decreases the time lapse between live imaging and the fixed sample state for EM to the order of milliseconds, or the time needed for the sample to cool. (A) Live imaging, cryofixation and cryo-light microscopy are integrated into a single system. The integrated system is then connected to electron microscopy. (B) *In situ* microfluidic cryofixation. A PDMS microfluidic channel is mounted onto a thin film resistive heater. The resistive heater is in thermal contact with a liquid nitrogen cooled heat sink. The heater preserves the sample of interest at room temperature in the microchannel during live imaging. When the heater is turned off, the contents of the channel cool rapidly and the sample is cryofixed within the field of view of the microscope.

thermal energy that must be dissipated by the heat sink. The microscale critical dimensions and low thermal mass make the system a viable tool for cryofixation (Mejia *et al.*, 2014) assessed below by the preservation of sample ultrastructure in TEM images. However, with an effective size of up to 40 μm (15 μm channel bottom + 25 μm sample/media), the system reported here requires the addition of cryoprotectants for sample ultrastructure preservation (Studer *et al.*, 1995; Mejia *et al.*, 2014).

The *in situ* cryofixation system is designed as a self-contained, modular microscopy stage (Fig. 2). With this design, the sample can be transferred while in contact with the cold heat sink, enabling cryotransfer following cryofixation. The main heater responsible for temperature control within the microchannel is thermally connected to the heat sink by a cold copper post. The microfluidic device, composed of the main PDMS microchannel and a silicon injector chip, is aligned and mounted onto the main heater.

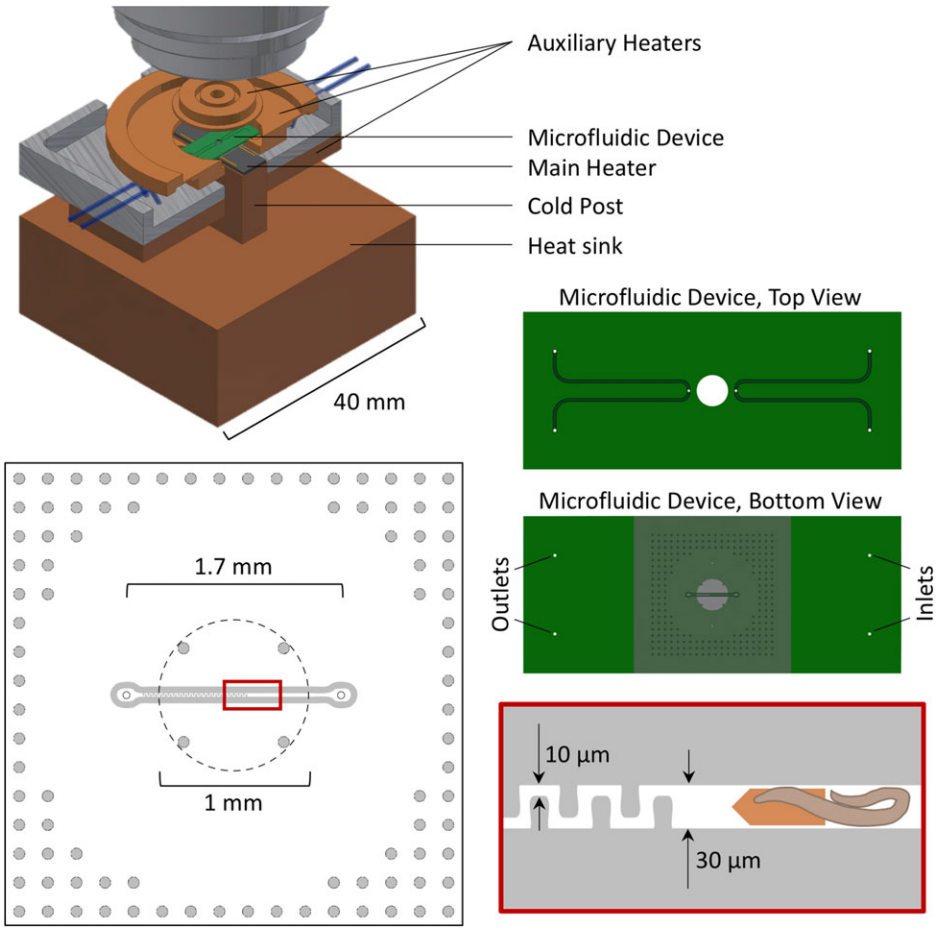

Fig. 2. *In situ* cryofixation system. The modular system design facilitates sample transfer at cryotemperature following *in situ* cryofixation (see Supporting Information for sample transfer procedures). The cold post thermally connects the heat sink and the main heater. The microfluidic device (green) is aligned and brought into contact with the main heater. Auxiliary heaters ensure the full fluidic network remains heated and flowing up until the moment of cryofixation. The microfluidic device consists of a silicon injector chip (green) and a PDMS microchannel, which contains the sample of interest. The main PDMS microchannel forms part of a 5 mm × 5 mm PDMS foil. An air gap surrounds the microchannel to reduce the overall thermal mass and thus increase the sample cooling rate. The array of microposts on the foil provides mechanical support that prevents excessive loading of the microchannel walls in the fully assembled system. The PDMS foil is bonded to the bottom side of the silicon injector chip to form the microfluidic device. One millimetre of the 1.7 mm long microchannel is suspended across the view window in the silicon, serving the dual purpose of making the sample visible and reducing the thermal mass. The silicon injector chip is used to introduce the sample into the PDMS microchannel. Fluidic tubing (0.8 mm outer diameter) connects to the injector chip inlets and outlets. The sample enters the injector chip by the inlet ports etched through the silicon (bottom of microfluidic device) and flows through the U-shaped bypass channels (top of microfluidic device) into the main PDMS microchannel. At the centre of the field of view, the channel width narrows from 30 to 10 μm and the straight channel becomes a zigzag structure. Although *C. elegans* can be pushed into the zigzag structure by sufficiently high pressure, the worms cannot enter the structure independently as the geometry prevents body bending. The trapping structures block *C. elegans* migration to the left whereas minimal pressure driven flow prevents the nematode from migrating to the right. The orange arrow denotes the direction of the flow.

In the fully assembled system, the sample of interest is visible within the microchannel through a 1 mm diameter view window in the silicon injector chip. Here, L1 *C. elegans*, with a body diameter of ~12 μm, was selected as a model system. *C. elegans* is a popular model system for genetics, neuroscience and developmental biology (Brenner, 1974; Sulston & Horvitz, 1977; White *et al.*, 1986; Bargmann, 1998; Fire *et al.*, 1998; The C. elegans Sequencing Consortium, 1998). As a simple, multicellular eukaryotic organism with a well-defined nervous system, *C. elegans* allows investigation of the underlying molecular and cellular mechanisms that relate to animal behaviour (Schafer, 2005; Urmersbach *et al.*, 2016). As correlative light and electron microscopy links structure to function, it is a well-suited technique for *C. elegans* studies (Bert *et al.*, 2016; Karreman *et al.*, 2016).

Trapping structures were incorporated into the microchannel to facilitate positioning of the *C. elegans* along the channel axis (Fig. 2). The traps maintain the nematode in the microscope field of view during live imaging without restricting typical body bending behaviour (see Supporting Information). To ensure nematode viability, the channel temperature was set within less than 2°C of the desired set-point using a temperature sensitive fluorescent probe (RhB-ITC-Dextran) prior to each experiment (see Supporting Information).

Cryofixation of C. elegans during live imaging

To establish a proof of principle for millisecond time-correlated live imaging and electron microscopy by *in situ* cryofixation, we injected L1 *C. elegans* into our microfluidic cryofixation system, recorded its movement up to the time of cryofixation and then imaged sections of the worm by TEM. Figure 3 shows images extracted from a 10 frames per second (fps) video of a *C. elegans* within the microchannel. The nematode was suspended in M9 with 10% (m/m) trehalose added as a cryoprotectant. The *C. elegans* here are genetically modified to express the calcium indicator GCaMP3.35 in striated body wall muscles (Schwarz *et al.*, 2012). Neural excitation triggers transient changes in intracellular calcium concentration, leading to a local increase in GCaMP fluorescence intensity during muscle contraction, as seen in Figure 3. Because a 510 nm long pass emission filter was used, autofluorescent gut granules were also observed during fluorescence imaging.

Cryofixation was triggered during a mid-body muscle contraction, arresting the nematode within the microscope field of view. To our knowledge, the live video of *Caenorhabditis elegans* cryofixation is the first demonstration of *in situ* cryoarrest within milliseconds. Panels 4 and 5 show the *C. elegans* before and after cryofixation, respectively. In Figure 3, a 10 fps frame rate was used to ensure an appreciable fluorescence signal. A bright field video of a different *C. elegans* cryofixation recorded at 100 fps is given in the Supporting Information. From the

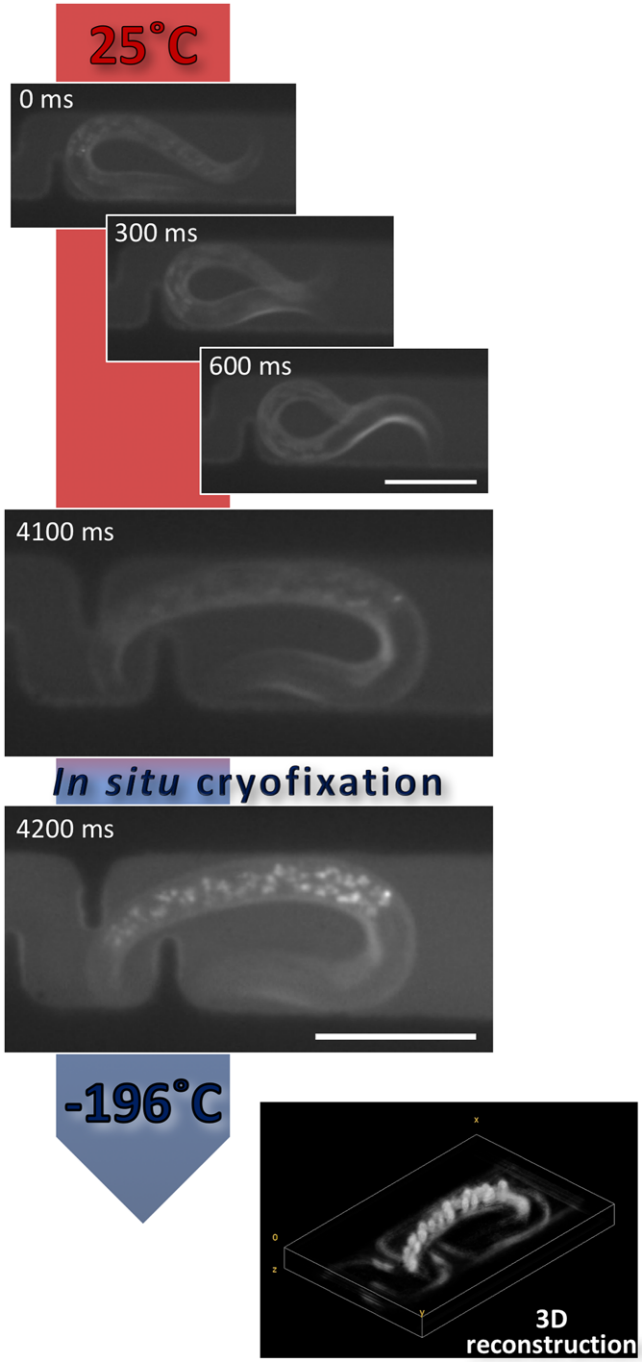

Fig. 3. Images extracted from a 10 fps video of *C. elegans* cryofixation during calcium imaging. Cryofixation was triggered during a mid-body muscle contraction. Panels 1–4 (0–4100 ms) and Panels 5–6 (4200 ms and 3D) show the nematode before and after cryofixation respectively. The *C. elegans* was suspended in M9 with 10% (m/m) trehalose added as a cryoprotectant. Images for the volume reconstruction were taken under cryoconditions. With the sample cryoarrested, exposure time can be increased beyond the time of the event itself, as in the 3D reconstruction, where the total 2.6-s exposure for the image stack far exceeds the time for a body bend. Imaging was performed using a 20×/0.40NA air objective with 3.9 mm working distance. The scale bar is 30 μm.

higher frame rate video, the *C. elegans* stops moving and the channel contents solidfy within three video frames (see Supporting Information), or within 30 ms.

Connecting in situ cryofixation to electron microscopy

The modular design of our microfluidic cryofixation stage enables the frozen sample to be transferred at cryotemperature from the light microscope to liquid nitrogen storage. During live imaging, the copper heat sink is partially submerged in a liquid nitrogen-filled cryobath (Fig. S3). Following *in situ* cryofixation, the entire assembly (Fig. 2) is transferred from the testing system into a dewar, where it is submerged under LN_2. It is critical that the sample temperature remains below –140°C during all transfer steps to avoid ice recrystallisation. Due to the size of the heat sink, the temperature of the assembly remains below –190°C during transfer with no measurable temperature increase between removal from the testing system and immersion in LN_2 (Fig. S4). Removing a single retaining ring allows sample recovery under LN_2 with LN_2 cooled forceps. The microfluidic device is then stored under LN_2 in a vented cryovial until further processing.

Microfluidic cryofixation was found to be compatible with freeze substitution and resin embedding protocols for room temperature electron microscopy (Cavalier *et al.*, 2009). The microchannel was accessed by scoring the ends of the channel outside of the 1 mm diameter view window under LN_2 prior to freeze substitution. Freeze substitution was then performed with a Leica EM AFS according to usual procedures, as described in the materials and methods.

Figure 4 shows the same *C. elegans* in light and electron microscopy with an effective millisecond scale time-lapse between the images. We assessed the quality of the sample preservation using the microfluidic cryofixation method by TEM of freeze substituted and resin embedded sections of *C. elegans*. The *C. elegans* was suspended in M9 medium with 10% (m/m) glycerol as a cryoprotectant prior to cryofixation. Overall, the TEM images reveal that *C. elegans* ultrastructure was well preserved, with smooth, well-defined membranes. The nematode is free from vacancies that would indicate crystalline ice damage. On closer inspection, the higher-magnification inset in Figure 4 illustrates a nucleus with visible nuclear pores and minimal segregation patterns from ice crystallisation. Generally, ultrastructure deformation is not noted throughout the nematode section with the exception of the nuclei, whose reticulated appearance in some locations is characteristic of crystalline ice damage. It cannot be concluded, however, to which extent damage occurred during cryofixation or freeze substitution procedures (Brown *et al.*, 2009).

Discussion

Millisecond time correlated live imaging and electron microscopy is a fundamental advance towards real-time selection and arrest of a desired state in order to investigate dynamic biological processes across length scales. With that goal in mind, the *in situ* cryofixation system design provides unique capabilities for sample manipulation and observation prior to cryofixation. Heat transfer was optimised to warm the 3D microfluidic network, ensuring continuous flow of medium until the moment of cryofixation (see Supporting Information). This feature is unique to this cryofixation system and can be exploited to exchange the sample, introduce reagents, apply shear stress, and otherwise manipulate the experimental conditions. The effects of environmental variations can be continuously monitored with the light microscope, opening

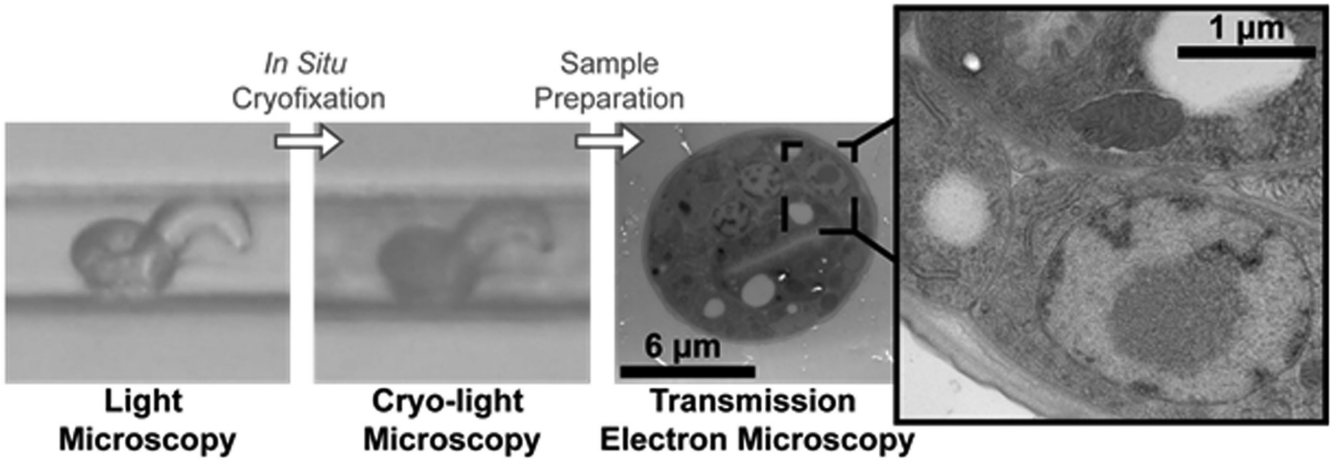

Fig. 4. Millisecond time correlated light and electron microscopy. The *C. elegans*, suspended in M9 with 10% (m/m) glycerol as a cryoprotectant, was cryofixed within the field of view of the light microscope. Transmission electron microscopy images of the same nematode indicate that overall the ultrastructure was well-preserved using *in situ* microfluidic cryofixation, however, varying degrees of crystalline ice damage were observed in the nuclei. The Supporting Information includes further transmission electron microscopy images as well as larger versions of the TEM images shown here.

the possibility to select and arrest a desired state for high-resolution imaging.

In addition to correlating light and electron microscopy, the *in situ* cryofixation system permits the correlation of other imaging modalities in which cryogenic operation is advantageous. Cryoarresting the sample permits, for example, longer exposure times in fluorescence microscopy to increase photon collection without bleaching, phototoxic side effects, or artefacts from sample dynamics (Kaufmann *et al.*, 2014; Masip *et al.*, 2016). As many fluorophores emit orders of magnitude more photons at cryogenic temperature than at room temperature (Kaufmann *et al.*, 2014; Li *et al.*, 2015; Weisenburger *et al.*, 2017), localisation microscopy can achieve significant resolution improvements under cryogenic conditions (Li *et al.*, 2015; Weisenburger *et al.*, 2017). Future work may include sample transfer from our system to super resolution-enabled cryofluorescence microscopes, which would be an ideal complement to ultrastructural imaging by EM due to the specificity of fluorescent tagging.

In situ cryofixation inherently provides a direct transition between live imaging and cryo-light microscopy within milliseconds. In future work, we plan to better exploit this characteristic by optimising the spatial resolution of our setup for both live imaging and subsequent cryo-light microscopy. One fundamental limitation of *in situ* cryofixation is that only air objectives can be used during the live imaging phase. Immersion objectives, which are often employed in confocal and super resolution microscopy, would interfere with the rapid cooling due to the thermal inertia of the immersion medium. Once frozen, however, the object could be imaged without restrictions using dedicated cryoimmersion objectives (Faoro *et al.*, 2018).

A second limitation for live imaging is that the current design of our cryofixation system requires a minimum working distance of 2.5 mm. In practice this is not a strong limitation, as long working distance high-NA objectives are readily available (e.g. the Mitutoyo 50 × 0.75 NA). With more advanced designs, a minimum working distance below 0.5 mm could likely be achieved, making a wider selection of high-NA air objectives available for live imaging and subsequent cryofixation (e.g. Mitutoyo 100 × 0.9 NA with a working distance of 1.3 mm). Further improvements will focus on optimisation of our cryofixation stage for mechanical stability and on methods to enable the precise spatial correlation of light and electron microscopy images of *in situ* cryofixed objects.

Sample size and tolerance to cryoprotectants determine the applicability of our system to specific samples. Given our current design, the combined size of the microchannel and the PDMS layer separating the channel from the heat sink is $\sim$40 μm. Therefore, the addition of cryoprotectants is necessary for ultrastructural preservation (Studer *et al.*, 1995; Mejia *et al.*, 2014). Here we have utilised 10% (m/m) trehalose or 10% (m/m) glycerol to cryofix *C. elegans*. *C. elegans* naturally produce trehalose in response to stressful environmental conditions (Chiu *et al.*, 2011), and glycerol is a well-established cryoprotectant for long term storage of *C. elegans* under liquid nitrogen. Other samples, however, may not tolerate an equivalent concentration of these cryoprotectants due to toxicity or reduced tolerance to osmotic stress compared to *C. elegans*. A suitable cryoprotectant type and minimum concentration needs to be assessed on a case by case basis depending on sample size, cryoprotectant type (permeant vs. nonpermeant), and sample type, as solute concentrations in the sample act as natural cryoprotectants (Studer *et al.*, 1995; Leforestier *et al.*, 1996; Erk *et al.*, 1998). Cryoprotectant choice should be referenced to a screening assay for cryoprotectant toxicity and tolerance to osmotic stress, which varies with molecular mass and concentration of the cryoprotectant (Pellerin-Mendes *et al.*, 1997; Reid *et al.*, 1997).

A main focus of future developments is to redesign the microfluidic device fabrication protocols to reduce the effective sample size (via both reduced bottom wall thickness and channel height) and minimise required cryoprotectant concentrations. COMSOL simulations from our previous work (Mejia *et al.*, 2014) indicate that under ideal conditions a cooling rate of 10^5–10^6 °C s^{-1} could be achieved throughout the depth of a 15 μm channel with a 0.5 μm bottom (effective sample size of 15.5 μm). This is similar to theoretical cooling rates for slam-freezing ($\sim 10^6$ °C s^{-1}), which also relies on one-sided heat conduction at atmospheric pressure (Heuser *et al.*, 1979; Studer *et al.*, 1995). Experimental results for slam-freezing report preservation for biological samples in the range of 10–15 μm without cryoprotectants (Heuser *et al.*, 1979; Leforestier *et al.*, 1996). Achievable results, however, can vary widely based on the water/solute content of the sample (Studer *et al.*, 1995; Leforestier *et al.*, 1996; Erk *et al.*, 1998) and the total sample thickness (i.e. thermal mass) (Escaig, 1982; Studer *et al.*, 1995), which determine the necessary cooling rate for vitrification.

In summary, we have described an approach to attain millisecond time correlated live imaging and electron microscopy by cryofixing the sample directly in the light microscope field of view. As a proof-of-principle, we demonstrated cryofixation of motile *Caenorhabditis elegans* roundworms during calcium imaging, monitored at video-rate. *C. elegans* was used as a model system to establish (i) compatibility of *in situ* microfluidic cryofixation with standard sample preparation techniques for electron microscopy and (ii) *in situ* cryofixation technology is capable of producing a well-preserved sample ultrastructure in EM. Previously reported approaches based on high-pressure freezing or plunge freezing require a transfer step between live imaging and cryofixation. Our approach improves the achievable time correlation of live imaging and electron microscopy by up to three orders of magnitude, from a limit lying in the order of seconds to milliseconds.

We expect that the ability to correlate live imaging and electron microscopy at the millisecond scale will enable new

paradigms based on real-time selection and arrest of a desired state to study biological processes across length scales. Continuous fluidic flow, a unique feature of this cryofixation system, can be exploited to manipulate the experimental conditions until the moment of cryofixation. The effects of environmental variations can be continuously monitored with the light microscope, opening the possibility to select and arrest a desired state for high-resolution imaging.

The general transfer procedures from *in situ* cryofixation to liquid nitrogen storage developed as part of this work can be readily extended to connect *in situ* cryofixation with other high-resolution imaging techniques. In future studies, we aim to connect *in situ* cryofixation to cryo-super resolution microscopy, room temperature FIB/SEM volume imaging, and to cryo-EM following cryo-FIB milling. We further seek to develop protocols for precise spatial correlation of light and electron microscopy images of *in situ* cryofixed objects.

Materials and methods

C. elegans strain HBR4: goeIs3[pmyo-3::GCamP3.35::unc-54–3′utr, unc-119(+)]V, expressing the green fluorescent protein calcium indicator GCaMP3.35 (Schwarz *et al.*, 2012), was used for the fluorescence/cryofluorescence imaging. *C. elegans* were grown on nematode growth medium (NGM) agarose plates seeded with *E. coli* OP50 and held at 20°C (Schwarz *et al.*, 2012). The *C. elegans* were suspended in M9 buffer with 10% (m/m) cryoprotectant (D(+)-trehalose dihydrate, Carl Roth GmbH + Co, Germany or glycerol, Invitrogen, CA, USA) and then introduced into the microchannel. The microfluidic device and NiCr resistive heater were fabricated similar to previously reported procedures (Mejia *et al.*, 2014).

Fluorescence microscopy was performed using a 20× air objective (0.4 NA) with a Nikon E-600 microscope and a Nikon IntensiLight mercury lamp. Microchannel temperature calibration was performed using DI water with 1% (m/m) Rhodamine B isothiocyanate–Dextran (RhB-ITC-Dextran 70 kDa, Sigma-Aldrich, MO, USA) according to procedures described in detail in the Supporting Information. For the temperature calibration, a 546/10 nm excitation and a 575 nm long pass emission filters were used whereas a 480/40 nm excitation filter and a 510 nm long-pass emission filter were used for fluorescence measurements of *C. elegans*. Fluorescence images in Figure 3 were acquired with an Andor Neo sCMOS camera. The volume reconstruction shown in Figure 3 was obtained using a 26-slice wide-field z-stack image, each slice taken 1 μm apart with a 100 ms exposure and successively deconvolved to remove out-of-focus light. Light and cryo-light microscopy images shown in Figure 4 were taken with a Canon EOS 700D digital camera fitted with an infinity-correction tube (Proximity series, InfiniTube, Infinity Photo-Optical Company, CO, USA) and a 10× air objective (0.2 NA).

C. elegans were freeze substituted at –90°C in anhydrous acetone with 0.1% tannic acid for 24 h and in anhydrous acetone, 2% OsO_4, 0.5% anhydrous glutaraldehyde (EMS Electron Microscopical Science, Ft. Washington, USA) for additional 8 h. After a further incubation over 20 h at –20°C samples were warmed up to +4°C and washed with anhydrous acetone subsequently, using a Leica EM AFS (Leica Mikrosysteme Vertrieb GmbH, Wetzlar, Germany). The 5 mm × 5 mm PDMS foil containing the freeze substituted sample was then mechanically removed from the silicon injector chip. Samples were then embedded in Agar 100 (Epon 812 equivalent) at 60°C over 24 h. The embedded sample was sectioned into ~70 nm thick sections with an ultramicrotome and visualised in CM120 TEM (Philips Inc. Eindhoven, the Netherlands).

Acknowledgements

The authors gratefully acknowledge the Max Planck Society for funding this work. The authors would like to thank Leica Microsystems for loan of supporting equipment. Henrik Bringmann is gratefully acknowledged for providing wild-type and GCaMP *C. elegans* strains, as well as for useful discussions regarding this work. The authors thank R.I. Galilea Kleinsteuber for assistance with experiments. M. Fuest would like to acknowledge funding from the European Union's Horizon 2020 research and innovation programme under the Marie Skłodowska-Curie Fellowship Program Project ID: 749830.

References

Al-Amoudi, A., Norlen, L.P.O. & Dubochet, J. (2004) Cryo-electron microscopy of vitreous sections of native biological cells and tissues. *J. Struct. Biol.* **148**(1), 131–135.

Bargmann, C.I. (1998) Neurobiology of the Caenorhabditis elegans genome. *Science* **282**(5396), 2028–2033.

Bert, W., Slos, D., Leroux, O. & Claeys, M. (2016) Cryo-fixation and associated developments in transmission electron microscopy: a cool future for nematology. *Nematology* **18**(1), 1–14.

de Boer, P., Hoogenboom, J.P. & Giepmans, B.N.G. (2015) Correlated light and electron microscopy: ultrastructure lights up! *Nat. Methods* **12**(6), 503–513.

Brenner, S. (1974) The genetics of Caernorhabditis elegans. *Genetics* **77**, 71–94.

Brown, E., Mantell, J., Carter, D., Tilly, G. & Verkade, P. (2009) Studying intracellular transport using high-pressure freezing and correlative light electron microscopy. *Semin. Cell. Dev. Biol.* **20**(8), 910–919.

Cavalier, A., Spehner, D. & Humbel, B.M. (2009) *Handbook of Cryo-Preparation Methods for Electron Microscopy*, Chapter 13. CRC Press, Boca Raton.

Chen, B. & Frank, J. (2016) Two promising future developments of cryo-EM: capturing short-lived states and mapping a continuum of states of a macromolecule. *Microscopy* **65**(1), 69–79.

Chiu, P.-L., Kelly, D.F. & Walz, T. (2011) The use of trehalose in the preparation of specimens for molecular electron microscopy. *Micron* **42**(8), 762–772.

Dubochet, J. (2012) Cryo-EM-the first thirty years. *J. Microsc.* **245**(3), 221–224.

Dubochet, J. & McDowall, A.W. (1981) Vitrification of pure water for electron microscopy. *J. Microsc.* **124**(3), 3–4.

Erk, I., Nicolas, G., Caroff, A. & Lepault, J. (1998) Electron microscopy of frozen biological objects: a study using cryosectioning and cryosubstitution. *J. Microsc.* **189**, 236–248.

Escaig, J. (1982) New instruments which facilitate rapid freezing at 83 K and 6 K. *J. Microsc.* **126**(3), 221–229.

Faoro, R., Bassu, M., Mejia, Y.X., Stephan, T., Dudani, N., Boeker, C., Jakobs, S. & Burg, T.P. (2018) Aberration-corrected cryoimmersion light microscopy. *PNAS* **115**(6), 1204–1209.

Fire, A., Xu, S., Montgomery, M.K., Kostas, S.A., Driver, S.E. & Mello, C.C. (1998) Potent and specific genetic interference by double-stranded RNA in Caenorhabditis Elegans. *Nature* **391**(6669), 806–811.

Gautier, A., Michel-Salamin, L., Tosi-Couture, E., McDowall, A.W. & Dubochet, J. (1986) Electron microscopy of the chromosomes of dinoflagellates in situ: confirmation of bouligand's liquid crystal hypothesis. *J. Ultrastruct. Mol. Struct. Res.* **97**(1–3), 10–30.

Heuser, J.E., Reese, T.S., Dennis, M.J., Jan, Y., Jan, L. & Evans, L. (1979) Synaptic vesicle exocytosis captured by quick freezing and correlated with quantal transmitter release. *J. Cell Biol.* **81**(2), 275–300.

Karreman, M.A., Hyenne, V., Schwab, Y. & Goetz, J.G. (2016) Intravital correlative microscopy: imaging life at the nanoscale. *Trends Cell Biol.* **26**(11), 848–863.

Kaufmann, R., Hagen, C. & Grünewald, K. (2014) Fluorescence cryomicroscopy: current challenges and prospects. *Curr. Opin. Chem. Biol.* **20**, 86–91.

Knoll, G., Braun, C. & Plattner, H. (1991) Quenched flow analysis of exocytosis in paramecium cells: time course, changes in membrane structure, and calcium requirements revealed after rapid mixing and rapid freezing of intact cells. *J. Cell Biol.* **113**(6), 1295–1304.

Koning, R.I., Faas, F.G., Boonekamp, M. *et al.* (2014) MAVIS: an integrated system for live microscopy and vitrification. *Ultramicroscopy* **143**, 67–76.

Leforestier, A., Richter, K., Livolant, F. & Dubochet, J. (1996) Comparison of slam-freezing and high-pressure freezing effects on the DNA cholesteric liquid crystalline structure. *J. Microsc.* **184**, 4–13.

Li, W., Stein, S.C., Gregor, I. & Enderlein, J. (2015) Ultra-stable and versatile widefield cryo-fluorescence microscope for single-molecule localization with sub-nanometer accuracy. *Opt. Express* **23**(3), 3770–3783.

Loussert Fonta, C. & Humbel, B.M. (2015) Correlative microscopy. *Arch. Biochem. Biophys.* **581**, 98–110.

Masip, M.E., Huebinger, J., Christmann, J., Sabet, O., Wehner, F., Konitsiotis, A., Fuhr, G.R. & Bastiaens, P.I.H. (2016) Reversible cryo-arrest for imaging molecules in living cells at high spatial resolution. *Nat. Methods* **13**(8), 665–672.

McDonald, K.L. (2009) A review of high-pressure freezing preparation techniques for correlative light and electron microscopy of the same cells and tissues. *J. Microsc.* **235**(3), 273–281.

McDonald, K. & Morphew, M.K. (1993) Improved preservation of ultrastructure in difficult-to-fix organisms by high pressure freezing and freeze substitution: I. *Drosophila melanogaster* andstrongylocentrotus purpuratus embryos. *Microsc. Res. Tech.* **24**(6), 465–473.

Mejia, Y.X., Feindt, H., Zhang, D., Steltenkamp, S. & Burg, T.P. (2014) Microfluidic cryofixation for correlative microscopy. *Lab Chip* **14**(17), 3281–3284.

Ménétret, J.-F., Hofmann, W., Schröder, R.R., Rapp, G. & Goody, R.S. (1991) Time-resolved cryo-electron microscopic study of the dissociation of actomyosin induced by photolysis of photolabile nucleotides. *J. Mol. Biol.* **219**(2), 139–144.

Moor, H. (1987) Theory and practice of high pressure freezing. *Cryotechniques in Biological Electron Microscopy* (ed. by R.A. Steinbrecht & K. Zierold), pp. 175–191. Springer Berlin Heidelberg, Berlin, Heidelberg.

Moor, H. & Riehle, U. (1968) Snap-freezing under high pressure: a new fixation technique for freeze-etching. *Electron Microscopy 1968* (ed. by D. Steve Bocciarelli), pp. 33–34. Proc. 4th Eur. Reg. Conf. Electron Microsc, Rome.

Müller-Reichert, T., Hohenberg, H., O'Toole, E.T. & Mcdonald, K. (2003) Cryoimmobilization and three-dimensional visualization of *C. elegans* ultrastructure. *J. Microsc.* **212**(1), 71–80.

Pellerin-Mendes, C., Million, L., Marchand-Arvier, M., Labrude, P. & Vigneron, C. (1997) In vitrostudy of the protective effect of trehalose and dextran during freezing of human red blood cells in liquid nitrogen. *Cryobiology* **35**(2), 173–186.

Plitzko, J.M., Rigort, A. & Leis, A. (2009) Correlative cryo-light microscopy and cryo-electron tomography: from cellular territories to molecular landscapes. *Curr. Opin. Biotechnol.* **20**(1), 83–89.

Reid, C., Rand, R.P. & Gennes, P.-G. (1997) Fits to osmotic pressure data. *Biophys. J.* **73**, 1692–1694.

Schafer, W.R. (2005) Deciphering the neural and molecular mechanisms of *C. elegans* behavior. *Curr. Biol.* **15**(17), R723–R729.

Schaffer, M., Mahamid, J., Engel, B.D., Laugks, T., Baumeister, W. & Plitzko, J.M. (2017) Optimized cryo-focused ion beam sample preparation aimed at in situ structural studies of membrane proteins. *J. Struct. Biol.* **197**(2), 73–82.

Schertel, A., Snaidero, N., Han, H.M., Ruhwedel, T., Laue, M., Grabenbauer, M. & Möbius, W. (2013) Cryo FIB-SEM: volume imaging of cellular ultrastructure in native frozen specimens. *J. Struct. Biol.* **184**(2), 355–360.

Schwarz, J., Spies, J.P. & Bringmann, H. (2012) Reduced muscle contraction and a relaxed posture during sleep-like lethargus. *Worm* **1**(1), 12–14.

Shaikh, T.R., Barnard, D., Meng, X. & Wagenknecht, T. (2009) Implementation of a flash-photolysis system for time-resolved cryo-electron microscopy. *J. Struct. Biol.* **165**, 184–189.

Stepanek, L. & Pigino, G. (2017) Millisecond time resolution correlative light and electron microscopy for dynamic cellular processes. *Methods Cell Biol.* **140**, 1–20.

Studer, D., Michel, M., Wohlwend, M., Hunizker, E.B. & Buschmann, M.D. (1995) Vitrification of articular cartilage by high-pressure freezing. *J. Microsc.* **179**(3), 321–322.

Sulston, J.E. & Horvitz, H.R. (1977) Post-embryonic cell lineages of the nematode, *Caenorhabditis elegans*. *Dev. Biol.* **56**(1), 110–156.

The C. elegans Sequencing Consortium. (1998) Genome sequence of the Nematode *C. Elegans*: a platform for investigating biology. *Science* **282**, 2012–2018.

Urmersbach, B., Besseling, J., Spies, J.P. & Bringmann, H. (2016) Automated analysis of sleep control via a single neuron active at sleep onset in *C. Elegans*. *Genesis* **54**(4), 212–219.

Verkade, P. (2008) Moving EM: the rapid transfer system as a new tool for correlative light and electron microscopy and high throughput for high-pressure freezing. *J. Microsc.* **230**(2), 317–328.

Watanabe, S., Rost, B.R., Camacho-Pérez, M., Davis, M.W., Söhl-Kielczynski, B., Rosenmund, C. & Jorgensen, E.M. (2013) Ultrafast endocytosis at mouse hippocampal synapses. *Nature* **504**(7479), 242–247.

Weisenburger, S., Boening, D., Schomburg, B., Giller, K., Becker, S., Griesinger, C. & Sandoghdar, V. (2017) Cryogenic optical localization provides 3D protein structure data with angstrom resolution. *Nat. Methods* **14**(2), 141–144.

Wendt-Gallitelli, M.-F. & Wolburg, H. (1984) Rapid freezing, cryosectioning, and X-Ray microanalysis on cardiac muscle preparations in defined functional states. *J. Electron Microsc. Tech.* **1**(2), 151–174.

White, J.G., Southgate, E., Thomson, J.N. & Brenner, S. (1986) The structure of the nervous system of the nematode caernorhabditis elegans. *Phil. Trans. R. Soc. Lond. B* **314**(1), 1–340.

Supporting Information

Additional supporting information may be found online in the Supporting Information section at the end of the article.

Fig. S1. Microchannel temperature calibration.

Fig. S2. Frames extracted from the Supporting Information video of *in situ* cryofixation of a *C. elegans.*

Fig. S3. Transfer of a cryofixed sample from the *in situ* cryofixation system to LN_2 storage.

Fig. S4. Assembly temperature during transfer from the *in situ* cryofixation system to the LN_2 dewar.

Fig. S5. A larger version of the image shown in Figure 4 of the main manuscript. The white dashed boxes indicate the areas where the following higher-magnification images were taken.

Fig. S6. A larger version of the inset shown in Figure 4 of the main manuscript.

Fig. S7. Higher-magnificent image of L1 C. elegans cross section. Chromatin segregation seen in the nucleus here was caused by ice crystallisation.

Video S1. A 100 fps video of *in situ* cryofixation of *C. elegans*.

